

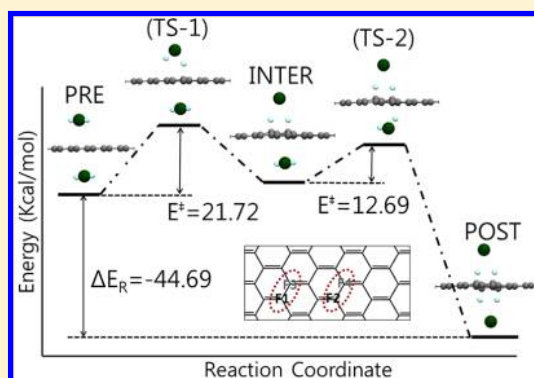
A Mechanistic Study of Graphene Fluorination

Sung-Sik Lee,[†] Sung-Woo Jang,[†] Kkochorong Park,[†] Eun Chong Jang,[†] Ju-Young Kim,[†] Daniel Neuhauser,^{*,‡} and Sungyul Lee^{*,†}

[†]Department of Applied Chemistry, Kyung Hee University, 1 Seocheon-dong, Giheung-gu, Yongin, Gyeonggi-do 446-701, Republic of Korea

[‡]Department of Chemistry and Biochemistry, University of California, Los Angeles, California 90095, United States

ABSTRACT: We describe the mechanism of graphene fluorination by XeF₂, calculated here by a periodic plane-wave DFT. We find that the fluorination of graphene proceeds by simultaneous bonding of two F atoms from XeF₂ via transition states that interact a bit asymmetrically with the graphene surface. The fluorination of graphene occurs at the (1, 4) positions of the constituent phenyl ring, eventually covering 25% of the graphene C atoms. Bonding to other positions involves large reaction barriers. We also elucidate the origin of experimental observations (Robinson, J. T.; et al. *Nano Lett.* **2010**, *10*, 3001) of 100% saturation with F when both sides are allowed to react with XeF₂. We find that fluorination at one side facilitates the bonding of F at the (1, 2) position on the other side of graphene by significantly lowering the activation barrier of fluorination, indicating that successive (1, 2) additions eventually lead to 100% coverage of graphene by F. We also discuss the effects of a defect on the graphene surface, proposing that two F atoms may bond to a site near a “missing” carbon atom.



INTRODUCTION

Graphene^{1–10} holds promise for applications in materials science, chemistry, biology, and medicine because of its unique physicochemical properties. Although the extreme chemical stability of graphene is the origin of its strong mechanical properties, it may hinder the use of the material for more diverse purposes. Thus it will be very important to modify and functionalize the inert graphene¹¹ as this may offer useful routes to design new materials with various electronic, optical, and chemical properties. Band gap engineering based on functionalizing graphene^{12–25} is a very important example of such processes. Although there have been numerous reports concerning this interesting subject, systematic study of the underlying mechanism is scarce.

Fluorination of graphene^{26–43} is quite amenable to such a mechanistic study, because it is simple enough for detailed quantum chemical analysis. Robinson and co-workers³⁰ reported recently that reaction with XeF₂ leads to partial or full fluorination of graphene, showing that the properties of graphene, such as the band gap, can vary considerably as a function of the degree of fluorination. The reaction of graphene surface with F was found to significantly depend on reaction conditions; only 25% coverage was observed when a single graphene surface is exposed to XeF₂, but full (100%) coverage emerged when both surfaces were allowed to react with XeF₂, with more than 100% coverage if defects are present.

Here we study the mechanism of fluorination of graphene by XeF₂ in order to elucidate these intriguing experimental observations. Calculations are carried out with a PAW-PBE pseudopotential, plane-wave basis and periodic boundary

conditions. The 25% coverage of one surface of graphene may well be described by successive fluorination at (1, 4) positions of the phenyl ring unit, whereas the 100% fluorination at both sides of graphene is elucidated by stepwise addition of XeF₂ at (1, 2) positions facilitated with lower barriers. As an attempt to understand more than 100% F coverage of graphene due to defects, we also discuss the effects of a “missing” carbon atom on the bonding of F atoms on graphene surface, suggesting that two F atoms may easily bond to a site near the defect with low reaction barrier (7–9 kcal/mol).

COMPUTATIONAL DETAILS

A periodic DFT method (GGA-PBE)^{44,45} is employed with a PAW-PBE⁴⁶ pseudopotential, a plane-wave basis, and $4 \times 4 \times 1$ k-point sampling with gamma point as implemented in the Vienna ab initio simulation package (VASP)^{47,48} suite of programs. In order to construct the graphene layer, we used a supercell consisting of 50 carbon atoms by adding 5 primitive cells with lattice constant 2.46 along the \vec{a} and \vec{b} axes with the length of 20 Å along the \vec{c} axis (see Scheme 1). Using larger cells did not give any significant changes to the results.

For pre/postreaction complexes, we apply the conjugate gradient algorithm with ionic relaxation. The density of state is obtained by employing a $24 \times 24 \times 1$ k-point sampling. The structures and energies of transition states are obtained by using

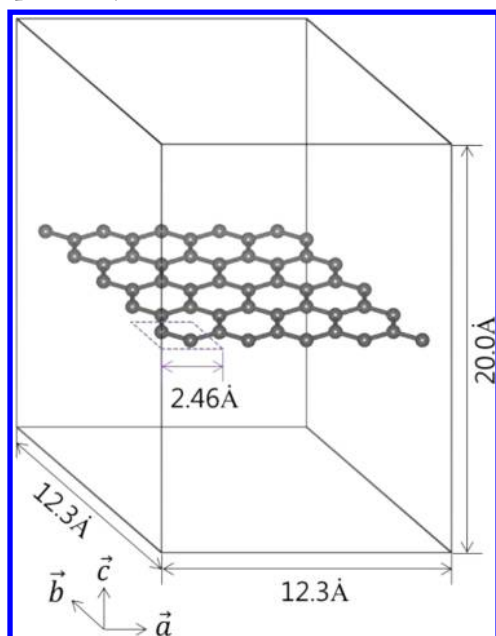
Received: November 1, 2012

Revised: February 21, 2013

Published: February 21, 2013



Scheme 1. Supercell Employed in This Work To Construct the Graphene Layer



the climbing image NEB (nudged elastic band) model and quick-minimum algorithm with five images between the pre- and post-reaction complexes. A smearing Gaussian of half-width 0.02 eV is applied. Hellman–Feynman forces of <0.02 and <0.1 eV/Å are employed to obtain the pre/postreaction complexes and the transition states, respectively. The electronic threshold of 10^{-7} is adopted for nonspin polarized calculations with the PREC=high option, and cutoff of 400 eV is used for pseudopotentials.

RESULTS AND DISCUSSION

The structures and energies of graphene–XeF₂ prereaction complexes (Pre-1)–(Pre-5) are presented in Figure 1 and Table 1.

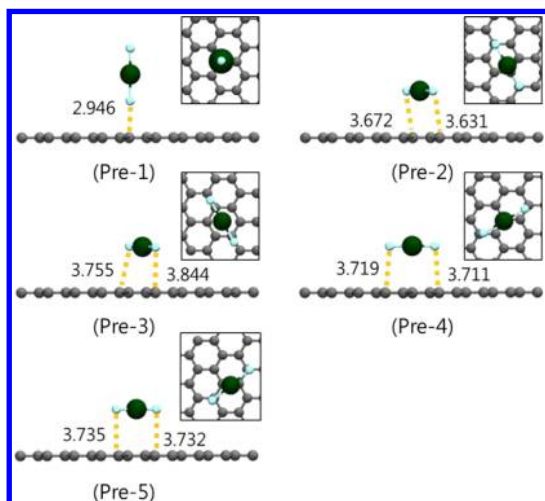


Figure 1. Side and top views of graphene–XeF₂ complexes.

The energies of the complexes are very close, the difference being ≤ 0.3 kcal/mol. The angle $\angle F-Xe-F$ and the distances R_{Xe-F} and R_{F-F} of the prereaction complexes are also quite similar, the differences mainly being in the R_{C-F} 's. In (Pre-1) XeF₂ binds perpendicular to graphene, whereas in other complexes it binds

more or less parallel to the graphene plane with F atoms interacting with two different carbon atoms. The R_{C-F1} distance (2.946 Å) in (Pre-1) is smaller than those (>3.6 Å) in complexes (Pre-2)–(Pre-5), probably because the bulky Xe does not interfere in the interaction between the graphene plane and a F atom in (Pre-1). The two R_{C-F} 's in (Pre-2)–(Pre-5) are a bit different, indicating that two F atoms in these complexes do not bind to the graphene plane in an equivalent fashion as depicted in the top views in Figure 1. The XeF₂ moiety remains essentially linear in these prereaction complexes.

The profiles and energetics of the reaction between XeF₂ and the graphene plane are presented in Figure 2. We find that (Pre-1) does not lead to fluorination, whereas structures (Pre-2)–(Pre-5) act as prereaction complexes for bonding of two F atoms on the surface of graphene with activation barriers of 21.0–22.6 kcal/mol via a single transition state. We find that the activation barrier of fluorination from (Pre-3) is lowest (21.0 kcal/mol), indicating that this process is favored kinetically. Since the reaction from (Pre-3) is exothermic ($\Delta E_R = -1.3$ kcal/mol), whereas those from other prereaction complexes are slightly endothermic ($<+4.5$ kcal/mol), the reaction from (Pre-3) is also favored thermodynamically. Due to small differences in E^\ddagger and ΔE_R , however, the fluorination processes from these complexes may compete in comparable ratios.

Structures of the postreaction complexes are also presented in Table 2 and Figure 2 a. In (Post-2) the two R_{C-F} 's are a slightly different (1.547, 1.578 Å), whereas they are identical in other postreaction complexes. The two Xe–F distances are slightly different (by 0.05–0.086 Å) in each complex. The F–Xe–F bond is highly bent with an angle of 67.5–108.4°. The positions of the two F atoms bonding to the graphene plane in the postreaction complexes are shown in Figure 2 c with their distances (4.4–5.8 Å) in Table 2. (Post-3) is calculated to be lowest in energy, while the energies of other postreaction complexes are higher by 1.8–5.4 kcal/mol.

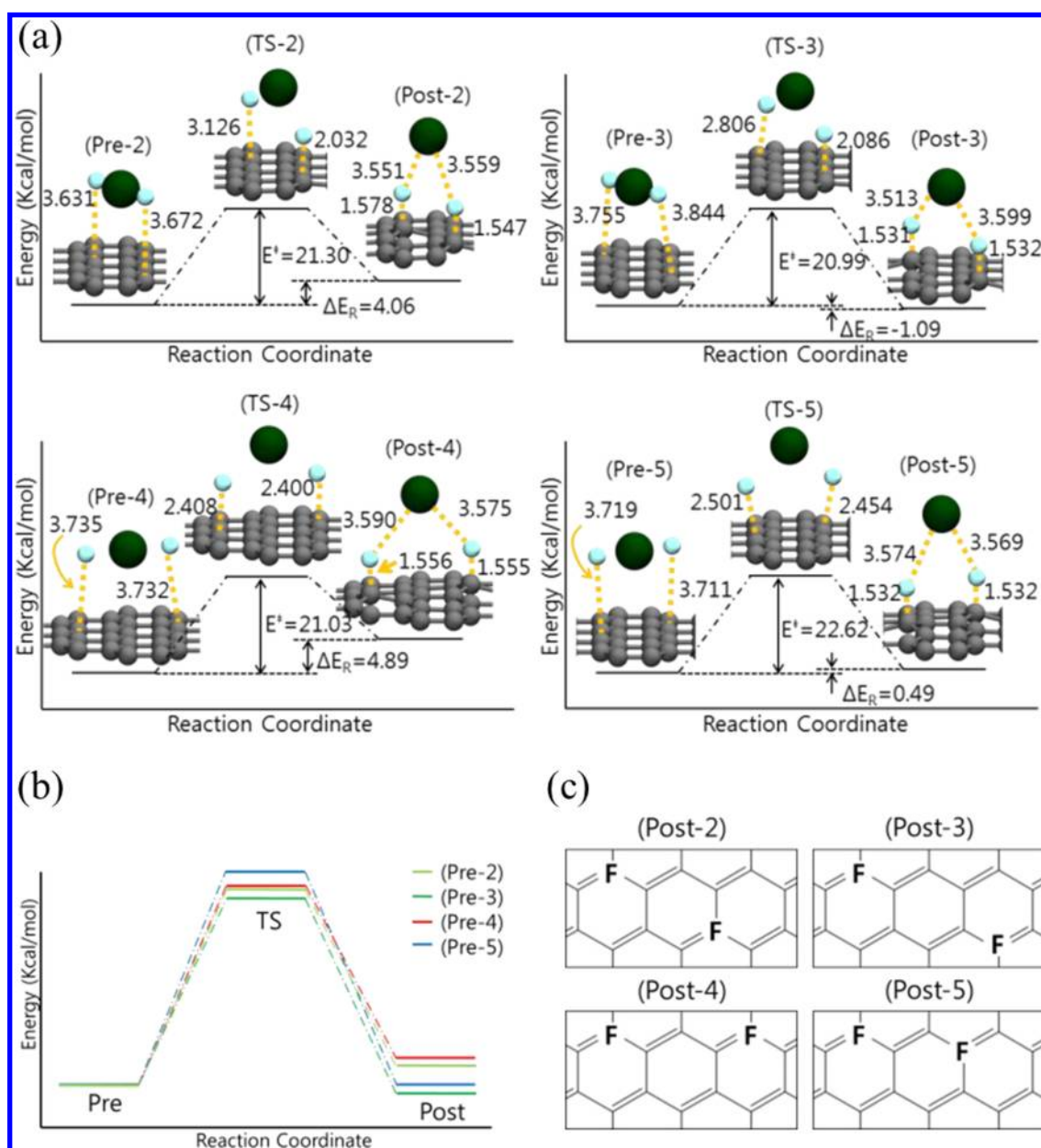
In Figure 3 we present and compare the density of state (DOS) of graphene and the graphene–XeF₂ postreaction complex (Post-3) by matching the Dirac points of graphene and (Post-3) with the Fermi level of (Post-3) as the zero of energy. The projected DOS shows that the p_z state in the conduction band at the C atom of graphene decreases after the reaction with XeF₂, whereas the p_x state in the valence band increases. This indicates that the unoccupied p_z state of graphene takes part in the reaction. On the other hand, the p_x state does not change much, because it partakes in C–C bonding as a state in valence band.

In Robinson and co-workers' experimental work,³⁰ it was reported that the coverage of F saturates at 25% when only one side of graphene surface is allowed to react with XeF₂. This observation may be elucidated by noting in Figure 4 the relative energies of graphene–F₂ as a function of the F–F distance. As the two F atoms get closer, the energy increases first very slowly (from (a) to (b), F–F distance decreases from 7.105 to 3.074 Å) but rapidly increases as the F–F distance decreases to 2.892 Å in (c). Note that structure (b), in which the two F atoms bind to carbon atoms in (1, 4) positions, is equivalent to the 25% F-covered graphene C₄F. The results depicted in Figure 4 thus clearly indicate that fluorination at one surface of graphene favors F coverage of less than 25%, saturating to C₄F.

In Figure 5 we depict the two structures for the 25%-covered C₄F, in which the F atoms bind at (1, 4) positions. Structure (a) consists of hexagonal cells, whereas the constituting cells in (b) are square. Robinson and co-workers proposed structure

Table 1. Structures, Energies E (eV), and Relative Energies ΔE (kcal/mol) of Graphene–XeF₂ Complexes^a

	R_{C-F1}	R_{C-F2}	$\angle F-Xe-F$ (deg)	R_{Xe-F}	R_{F-F}	E	ΔE
(Pre-1)	2.946	—	179.8	2.095/2.095	4.183	−466.56213	0
(Pre-2)	3.631	3.672	179.3	2.070/2.071	4.141	−466.55032	0.27
(Pre-3)	3.755	3.844	179.7	2.072/2.071	4.142	−466.55993	0.05
(Pre-4)	3.735	3.732	179.5	2.071/2.071	4.142	−466.54888	0.31
(Pre-5)	3.719	3.711	179.7	2.070/2.070	4.139	−466.55025	0.27

^aDistances in Å.Figure 2. Reaction mechanism (distances in Å) and activation barriers (kcal/mol) of graphene fluorination by XeF₂. (a) Reaction profiles, activation barriers E^\ddagger , and energies of reaction ΔE_R in kcal/mol. (b) Energetics and (c) positions of F atoms in postreaction complexes.Table 2. Structures (Distances in Å), Energy E (eV), and Relative Energy ΔE (kcal/mol) of Postreaction complexes

	R_{C-F1}	R_{C-F2}	$\angle F-Xe-F$ (deg)	R_{Xe-F}	R_{F-F}	E	ΔE
(Post-2)	1.547	1.578	77.8	3.551/3.559	4.465	−466.37405	5.38
(Post-3)	1.531	1.532	108.4	3.513/3.599	5.770	−466.60716	0
(Post-4)	1.555	1.556	88.66	3.575/3.590	5.009	−466.33699	6.23
(Post-5)	1.532	1.532	67.5	3.574/3.569	3.914	−466.52887	1.81

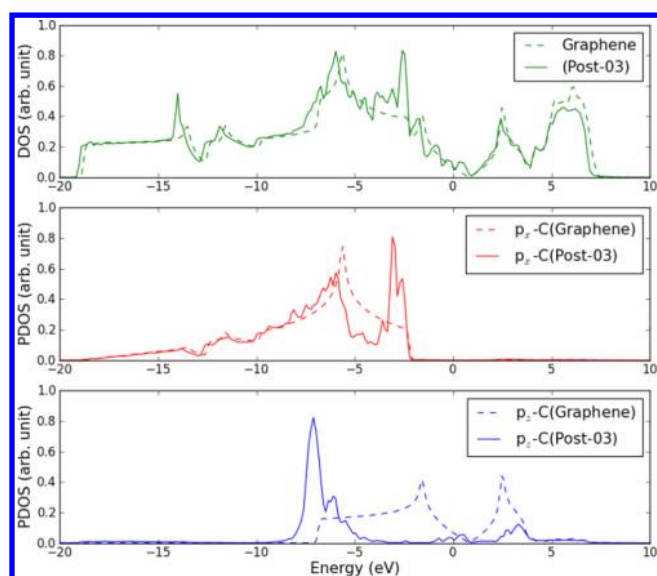


Figure 3. Changes in p_z and p_x states due to the reaction of graphene with XeF_2 .

(a) as the 25% F-covered graphene C_4F , and we also find that this structure is more stable than (b) by 16.4 kcal/mol. As indicated in Figure 5 a, this structure may be considered to arise from the prereaction complexes (Pre-3) and (Pre-4), but not from (Pre-2) or (Pre-5), with the F atoms located in honeycomb-like fashion. On the other hand, (b) corresponds to all prereaction complexes shown in Figure 1, except for (Pre-3).

In the transition state, F3 is closer than F4 to the graphene plane similarly to $[(\text{Post-2})-\text{XeF}_2]$. The activation barrier (19.4 kcal/mol) of the reaction $[(\text{Post-2}) + \text{XeF}_2 \rightarrow (\text{XeF}_2-$

graphene)- $\text{XeF}_2]$ is a bit smaller than that for $[(\text{Pre-2}) \rightarrow (\text{Post-2})]$, whereas for the reaction $[(\text{Post-3}) + \text{XeF}_2 \rightarrow (\text{XeF}_2-\text{graphene}-\text{XeF}_2)]$ it increases from 21.0 for the reaction $[(\text{Pre-3}) \rightarrow (\text{Post-3})]$ to 22.4 kcal/mol (Figure 6, Table 3). Although the reaction barrier from $[(\text{Post-2})-\text{XeF}_2]$ is lower than that from $[(\text{Post-3})-\text{XeF}_2]$, the energy of $[(\text{Post-3})-\text{XeF}_2]$ is lower than that for $[(\text{Post-2})-\text{XeF}_2]$ by 6.68 kcal/mol.

In Table 4 and Figure 7 we present four models based on the $[\text{XeF}_2 + \text{graphene}-\text{F}_2]$ system to describe the consecutive reactions of two XeF_2 molecules with graphene. In three of these, XeF_2 reacts at (1, 2), (1, 3), (1, 4) positions with $[\text{graphene}-\text{F}_2]$ that is formed by removing a Xe atom from (Post-2). The activation barriers for (1, 2), (1, 3), (1, 4) additions are 38.1, 31.7, 24.1 kcal/mol, respectively. Because the (1, 4) addition is equivalent to the situation depicted in Figure 5 b, the calculated lowest barrier for this process supports the experimental observation of 25% F coverage at a single side of graphene. In the fourth model (designated (1, 4)' in Figure 7), a pair of F atoms bind at (1, 4) positions at the graphene surface. The activation energy (26.9 kcal/mol) is 2.8 kcal/mol larger than that for (1, 4) addition listed in Table 4, but the energy of the (1, 4)' prereaction complex is lower than that for (1, 4) addition by 6.25 kcal/mol.

Robinson and co-workers³⁰ reported that graphene can be fully (100%) fluorinated when both sides of graphene surface are exposed to XeF_2 . In order to elucidate this intriguing observation, we calculate the activation barriers of the reaction of XeF_2 at the opposite side once a graphene surface is already fluorinated, in order to check whether this facilitates the reaction with XeF_2 on the other side. Our results presented in Figure 8 and Table 5 show that the reaction of two XeF_2 at the opposite sides of graphene is consecutive rather than concerted. The process involves an intermediate, in which a XeF_2 molecule has already

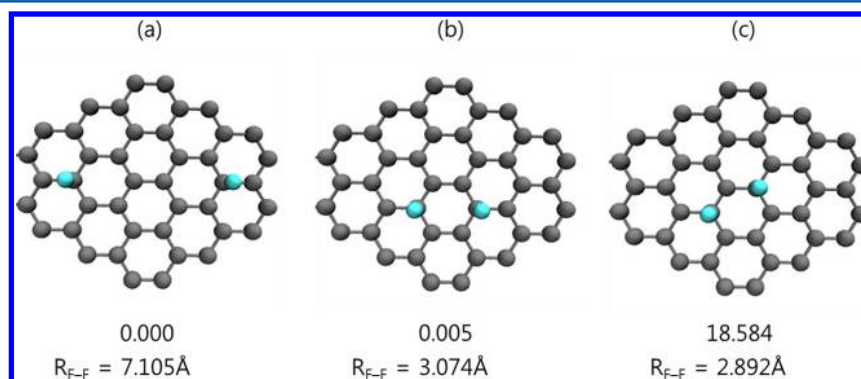


Figure 4. Relative energies (kcal/mol) of graphene- XeF_2 as a function of F-F distance on the surface of graphene.

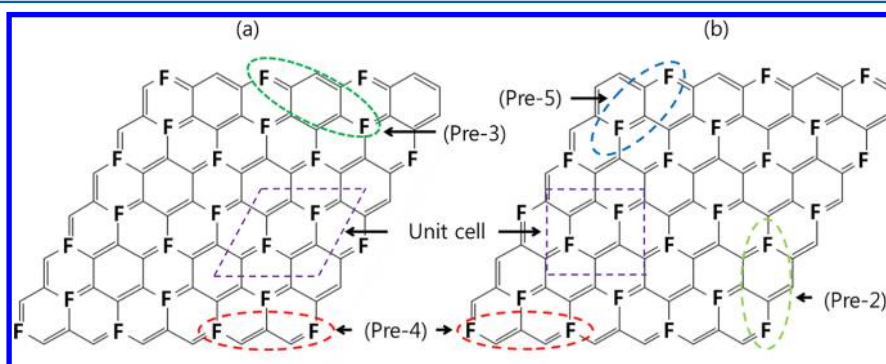


Figure 5. Structure (b) (bonding of two F atoms at (1, 4) positions) in Figure 4 is equivalent to 25% F-covered graphene, C_4F .

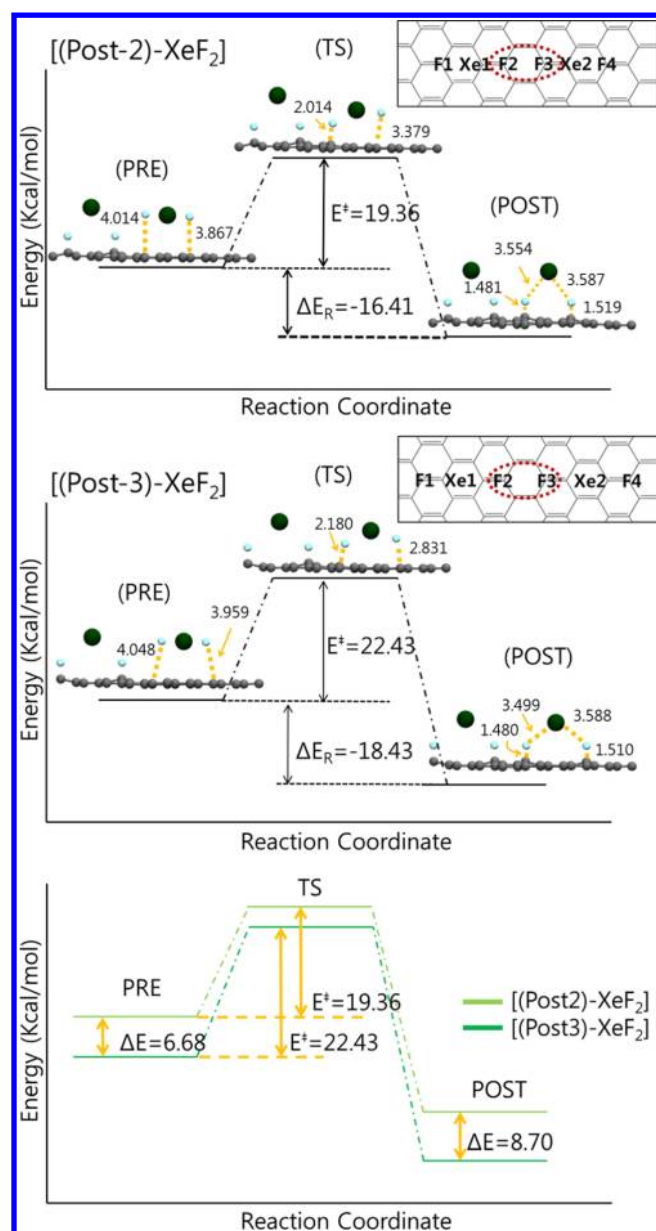


Figure 6. Mechanism and activation barriers of consecutive reactions of XeF_2 from the postreaction complexes (Post-2) and (Post-3).

reacted with a graphene surface, while another XeF_2 binds with the other side of graphene, ready for reaction. The reaction of XeF_2 with graphene in the first step [PRE \rightarrow (TS-1) \rightarrow INTER] is very similar to the reaction of (Pre-2) depicted in Figure 2 a,

with the activation barrier (21.7 kcal/mol) slightly higher (by 0.3 kcal/mol) than for the latter process. The bonding of two F atoms in the transition state (TS-1) is asymmetric as in the case of the reaction from (Pre-2). On the other hand, the activation barrier for the second step [INTER \rightarrow (TS-2) \rightarrow POST] is very low (12.7 kcal/mol), clearly indicating that the presence of a XeF_2 already bonding with graphene significantly facilitates the reaction of another XeF_2 molecule at the other side of graphene, with the nearest F atoms being in (1, 2) positions.

The bond distances $R_{\text{F1-C}}$ and $R_{\text{F2-C}}$ in the intermediates in (1, 2) and (1, 3) additions of two F atoms at opposite sides of graphene presented in Table 5 and Table 6, respectively, are quite similar, with differences $<0.002 \text{ \AA}$. This indicates that the positions of the second XeF_2 do not significantly affect the first (already reacted) XeF_2 . This may also be verified from the very similar energies of the two intermediates (the difference is only 0.548 kcal/mol).

As the second highly bent ($\angle\text{F3-Xe-F4} = 119.5^\circ$) XeF_2 approaches [graphene- XeF_2] in asymmetrical fashion in the transition state (TS-2), the $R_{\text{F1-C}}$ ($R_{\text{F2-C}}$) distance decreases from 1.545 (1.579) to 1.519 (1.532) \AA . The average F-C distance (1.559 \AA) in (1, 3) added XeF_2 -graphene- XeF_2 is larger than that (1.462 \AA) in the (1, 2)-added case. The activation barriers in the first [PRE \rightarrow (TS-1) \rightarrow INTER] and second [INTER \rightarrow (TS-2) \rightarrow POST] steps in this (1, 3) addition of two F atoms at opposite sides of graphene depicted in Figure 9 are 21.1 and 24.1 kcal/mol, respectively, a bit smaller than that ($E^\ddagger = 24.7 \text{ kcal/mol}$) in a (1, 4) addition of two F atoms on a single surface of graphene presented in Figure 7. It seems, however, that this process of (1, 3) addition at opposite sides of graphene is not favorable thermodynamically, because it is highly endothermic (overall $\Delta E_{\text{R}} = 14.7 \text{ kcal/mol}$). Although the successive fluorination at (1, 4) positions would not lead to 100% coverage of the two sides of graphene (it leaves some C atoms not bonding to F), we also study its mechanism and activation barriers to see whether it may contribute in part to the whole process. Figure 10 and Table 7 give the structures of pre/postreaction complexes and intermediate and transition states. The (1, 4) fluorination is a bit more advantageous both thermodynamically and kinetically over the (1, 3) process, with its barrier of 20.3 and 20.6 kcal/mol for the first and second reaction with XeF_2 and the reaction energy of -16.9 kcal/mol . It is, however, still much less favorable than the (1, 2) fluorination depicted in Figure 8. Therefore, we conclude that the 100% coverage of graphene by F atoms occurs via (1, 2) addition rather than (1, 3) or (1, 4) addition of F atoms.

Effects of the defects and imperfections are of great interest in relation to the physicochemical properties of graphene. Chemical environment near the defects would certainly differ from that of the perfect graphene surface, affecting the reactivity and electrical

Table 3. Comparison of Model Structures of C_4F Resulting from Consecutive Reaction of XeF_2 from the Postreaction Complexes (Post-2) and (Post-3)^a

	E	ΔE	$R_{\text{C-F1}}$	$R_{\text{C-F2}}$	$R_{\text{C-F3}}$	$R_{\text{C-F4}}$	$\angle\text{F1-Xe1-F2}(\text{deg})$	$\angle\text{F3-Xe2-F4}(\text{deg})$
(Post-2)- XeF_2								
PRE	-471.39311	0	1.553	1.560	4.014	3.867	79.5	179.2
TS	-470.55379	19.36	1.521	1.497	2.014	3.379	73.9	144.9
POST	-472.10472	-16.41	1.519	1.481	1.481	1.519	72.4	73.8
(Post-3)- XeF_2								
PRE	-471.68274	0	1.535	1.525	4.048	3.959	101.0	179.5
TS	-470.71002	22.43	1.507	1.489	2.180	2.831	99.7	135.8
POST	-472.48214	-18.43	1.510	1.481	1.480	1.510	98.7	104.9

^a Energy E in eV, relative energy ΔE in kcal/mol, and bond lengths in \AA .

Table 4. Energetics of the Reaction $\text{XeF}_2 + \text{Graphene}-\text{F}_2^a$

	E	ΔE	$R_{\text{F1-C}}$	$R_{\text{F2-C}}$	$R_{\text{F3-C}}$	$R_{\text{F4-C}}$	$\angle \text{F3-Xe-F4}$ (deg)
				(1, 2)			
PRE	-471.46280	0	1.531	1.617	4.811	4.842	177.7
TS	-469.81286	38.05	1.463	1.484	2.416	2.893	112.7
POST	-472.15521	-15.97	1.456	1.454	1.453	1.457	75.7
				(1, 3)			
PRE	-471.44204	0	1.544	1.579	4.056	4.065	177.1
TS	-470.06573	31.74	1.490	1.498	2.636	2.211	111.6
POST	-470.67531	17.68	1.523	1.540	1.525	1.542	75.2
				(1, 4)			
PRE	-471.46081	0	1.583	1.554	4.064	4.052	178.1
TS	-470.95967	24.13	1.494	1.519	1.883	3.562	143.8
POST	-472.27577	-18.79	1.481	1.486	1.453	1.482	74.1
				(1, 4)'			
PRE	-471.73168	0	1.556	1.526	3.892	4.044	179.0
TS	-470.56444	26.92	1.488	1.502	3.178	2.035	138.3
POST	-471.84772	-2.68	1.486	1.519	1.520	1.485	101.5

^aEnergy E in eV, relative energy ΔE in kcal/mol, and bond lengths in Å.

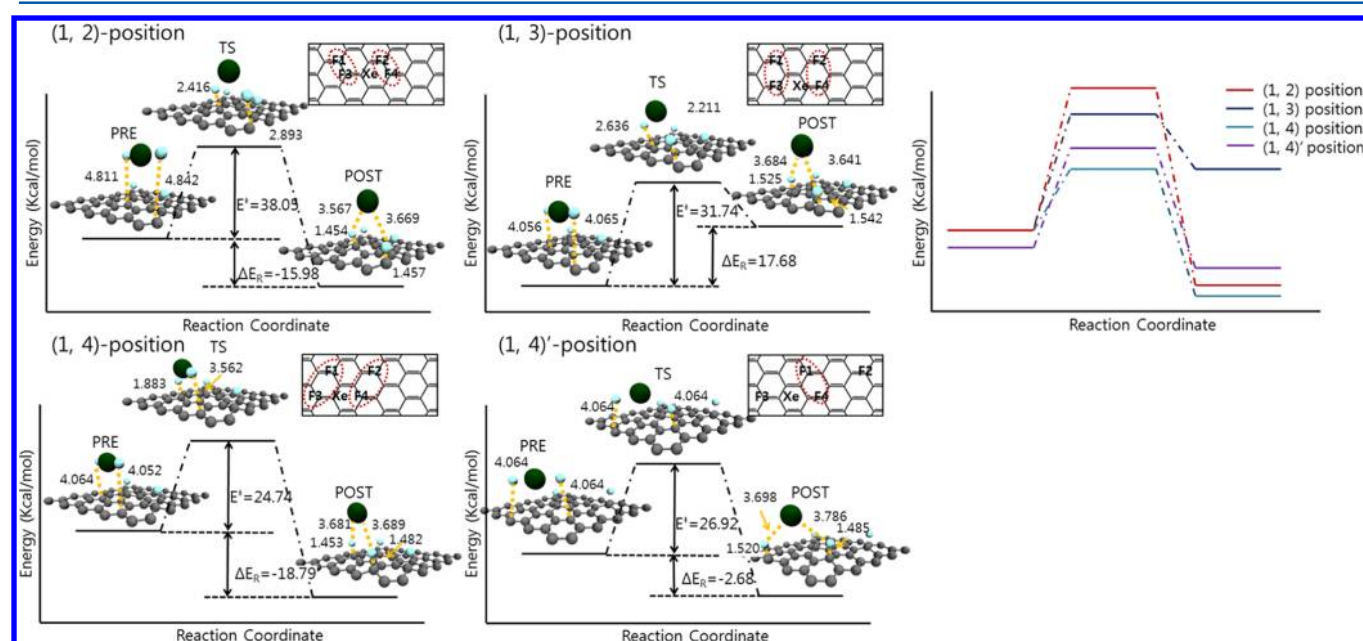


Figure 7. Profiles of the reaction $[\text{XeF}_2 + \text{graphene}-\text{F}_2]$. Energy in kcal/mol.

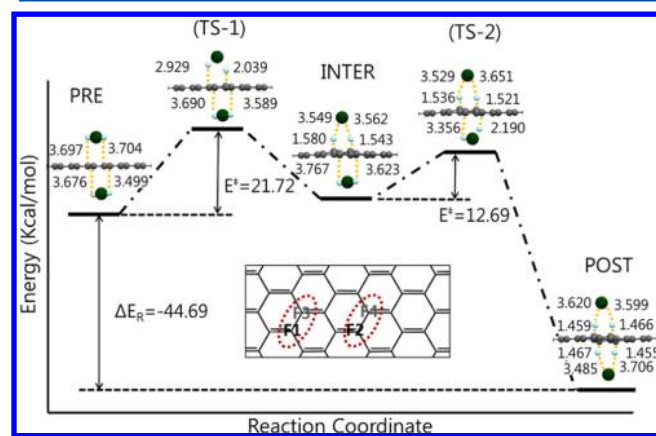


Figure 8. Profile and energetic of the reaction of two XeF_2 . Two nearest F atoms are at (1, 2) positions at opposite sides of graphene. Energy in kcal/mol and bond lengths in Å.

properties of graphene. In Robinson and co-workers' experimental work,³⁰ it was briefly commented that graphene may be oversaturated (more than 100% covered) by F due to defects or imperfections, presumably via C-F₂ type bonding. We treat the simplest type of defect and its effects on graphene fluorination by examining the reaction with XeF_2 near the site of a missing carbon atom on graphene surface.

In Figure 11 a, we present the reaction of XeF_2 at sites near a missing C of graphene. We find that the reaction with XeF_2 molecules proceeds very easily ($E^\ddagger = 8.7$ kcal/mol), as expected from the deficient valence of carbon atoms at the binding site. The defective graphene is constructed by removing a carbon atom from C₅₀. Figure 11 a shows that a carbon atom near the defect is a bit displaced from the plane of graphene. The $R_{\text{F1-C}}$ and $R_{\text{F2-C}}$ distances in the pre-reaction complex are 3.518 and 3.592 Å, respectively, somewhat shorter than those in (Post-3). In the transition state, $R_{\text{C-F1}}$ and $R_{\text{C-F2}}$ are 2.258, 3.451 Å, respectively, indicating that XeF_2 binds asymmetrically. In the

Table 5. Structures in the Reaction of Two XeF₂ with Both Sides of Graphene^a

	<i>E</i>	ΔE	R_{F1-C}/R_{F2-C}	R_{F3-C}/R_{F4-C}	R_{F1-Xe}/R_{Xe-F2}	R_{F3-Xe}/R_{Xe-F4}	$\angle F1-Xe-F2$ (deg)	$\angle F3-Xe-F4$ (deg)
PRE	-471.60700	0	3.704/3.697	3.499/3.676	2.070/2.069	2.070/2.071	179.6	179.6
(TS-1)	-470.66535	21.7	2.029/2.939	3.589/3.690	2.880/2.540	2.068/2.068	120.1	179.4
INTER	-471.45891	3.4	1.543/1.580	3.623/3.767	3.562/3.549	2.070/2.070	78.2	179.6
(TS-2)	-470.90862	16.1	1.521/1.536	2.190/3.356	3.651/3.529	2.511/2.331	75.2	146.1
POST	-473.54475	-44.7	1.466/1.459	1.455/1.467	3.599/3.620	3.706/3.485	73.3	73.6

^aEnergy *E* in eV, relative energy ΔE in kcal/mol, and bond lengths in Å. Two nearest F atoms are in (1, 2) positions at the opposite sides of graphene.

Table 6. Structures in the Reaction of Two XeF₂^a

	<i>E</i>	ΔE	R_{F1-C}/R_{F2-C}	R_{F3-C}/R_{F4-C}	R_{F1-Xe}/R_{Xe-F2}	R_{F3-Xe}/R_{Xe-F4}	$\angle F1-Xe-F2$ (deg)	$\angle F3-Xe-F4$ (deg)
PRE	-471.60219	0	3.703/3.700	3.536/3.701	2.069/2.070	2.071/2.071	179.8	179.7
TS1	-470.68663	21.1	1.969/3.028	3.634/3.742	2.868/2.532	2.066/2.067	123.5	179.1
INTER	-471.43513	3.9	1.545/1.579	3.686/3.520	3.561/3.552	2.066/2.068	78.2	179.4
TS2	-470.39124	27.9	1.519/1.532	2.631/2.348	3.568/3.548	2.683/2.739	76.6	119.5
POST	-470.96343	14.7	1.548/1.566	1.551/1.571	3.547/3.517	3.598/3.618	77.4	74.5

^aThe two nearest F atoms are in (1, 3) positions at opposite sides of graphene. Energy *E* in eV, relative energy ΔE in kcal/mol, and bond lengths in Å.

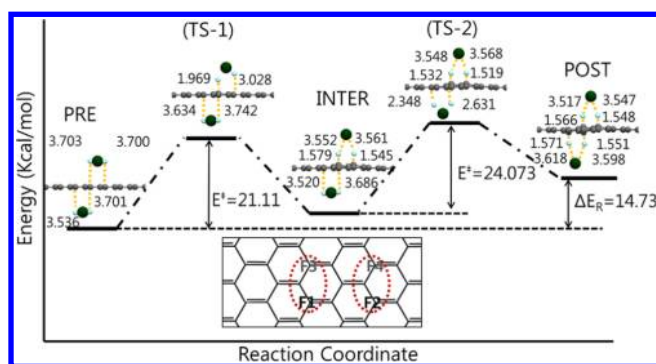


Figure 9. Profile and energetics of the reaction of two XeF₂. The two nearest F atoms are in the (1, 3) positions at opposite sides of graphene. Energy in kcal/mol and bond lengths in Å.

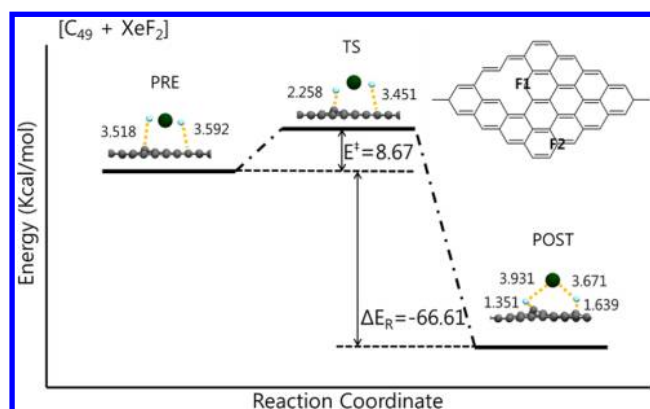


Figure 11. Mechanism and energy profile of the reaction C₄₉ + XeF₂ near a missing C atom of graphene.

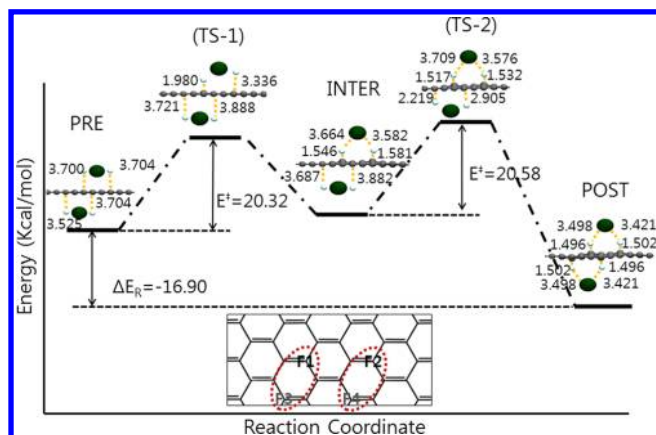


Figure 10. Profile and energetics of the reaction of two XeF₂. The two nearest F atoms are in the (1, 4) positions at opposite sides of graphene. Energy in kcal/mol and bond lengths in Å.

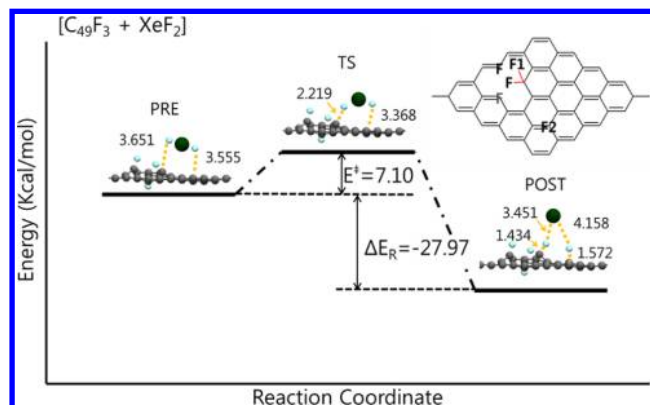


Figure 12. Mechanism and energy profile of the reaction C₄₉F₃ + XeF₂.

postreaction complex, the F atom is oriented obliquely toward the missing C, with R_{C-F1} of 1.351 Å. The reaction is highly exothermic ($\Delta E_R = -66.6$ kcal/mol).

Figure 12 depicts the reaction of XeF₂ with graphene in which three F atoms have already been added at sites near the missing C atom. As a result of the reaction with XeF₂, one of the carbon

atoms nearest to the defect now binds with two F atoms. The activation barrier (7.1 kcal/mol) is very low, and the reaction is highly exothermic again ($\Delta E_R = -28.0$ kcal/mol). Bonding with two F atoms makes the local structure at the C site essentially tetrahedral, exhibiting the sp³ type of bonding. The structure of oversaturated graphene C₄₉F₅₀ is depicted in Figure 13.

Table 7. Structures in the Reaction of Two XeF₂^a

	<i>E</i>	ΔE	R_{F1-C}/R_{F2-C}	R_{F3-C}/R_{F4-C}	R_{F1-Xe}/R_{Xe-F2}	R_{F3-Xe}/R_{Xe-F4}	$\angle F1-Xe-F2$ (deg)	$\angle F3-Xe-F4$ (deg)
PRE	-471.60347	0	3.700/3.704	3.525/3.704	2.070/2.069	2.070/2.070	179.8	179.7
TS1	-470.72241	20.3	1.980/3.336	3.721/3.888	2.851/2.492	2.067/2.066	127.7	179.3
INTER	-471.46739	3.1	1.546/1.581	3.687/3.882	3.664/3.582	2.067/2.066	76.3	179.3
TS2	-470.57519	23.7	1.517/1.532	2.219/2.905	3.709/3.576	2.624/2.445	74.3	130.6
POST	-470.33646	-16.9	1.496/1.502	1.502/1.496	3.690/3.543	3.498/3.421	73.7	77.6

^aThe two nearest F atoms are in (1, 4) positions at opposite sides of graphene. Energy *E* in eV, relative energy ΔE in kcal/mol, and bond lengths in Å.

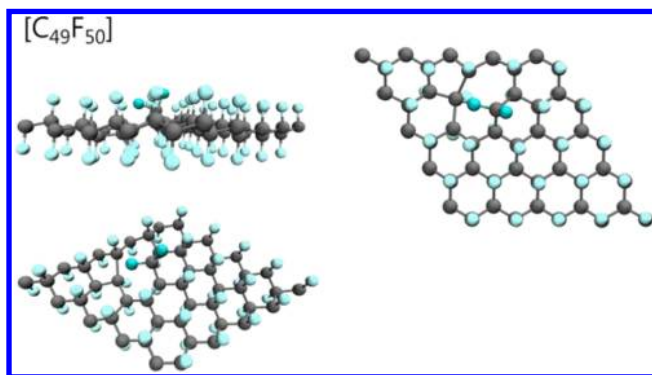


Figure 13. Oversaturation with F of graphene with a missing C atom: C₄₉F₅₀.

CONCLUSION

Our findings for the underlying mechanism of different coverage (25% at one side, full coverage at both surfaces of graphene and the effects of a defect) describe the process of graphene fluorination in molecular detail. Mechanistic study such as that presented here would be very helpful for understanding the nature of interactions and reactions on metal, semiconductor, and graphene surfaces. Fluorination of graphene has also proved to be instrumental for modifying and functionalizing graphene with a variety of bio/organic molecules. Further works, both experimental and theoretical, on this interesting subject would be highly desirable.

AUTHOR INFORMATION

Corresponding Author

* E-mail address: sylee@khu.ac.kr (S.L.); dxn@chem.ucla.edu (D.N.).

Notes

The authors declare no competing financial interest.

ACKNOWLEDGMENTS

Support by Kyung Hee University (2011) and by the Korea Research Foundation (2012-R1A2A2A02013289) is gratefully acknowledged.

REFERENCES

- (1) Novoselov, K. S.; Geim, A. K.; Morozov, S. V.; Jiang, D.; Zhang, Y.; Dubonos, S. V.; Grigorieva, I. V.; Firsov, A. A. Electric Field Effect in Atomically Thin Carbon Films. *Science* **2004**, *306*, 666–669.
- (2) Geim, A. K.; Novoselov, K. S. The Rise of Graphene. *Nat. Mater.* **2007**, *6*, 183–191.
- (3) Zhang, Y.; Tan, J. W.; Stormer, H. L.; Kim, P. Experimental Observation of the Quantum Hall Effect and Berry's Phase in Graphene. *Nature* **2005**, *438*, 201–204.
- (4) Service, R. F. Carbon Sheets an Atom Thick Give Rise to Graphene Dreams. *Science* **2009**, *324*, 875–877.

(5) Geim, A. K. Graphene: Status and Prospects. *Science* **2009**, *19*, 1530–1534.

(6) Lee, C.; Wei, X.; Kysar, J. W.; Hone, J. Measurement of the Elastic Properties and Intrinsic Strength of Monolayer Graphene. *Science* **2008**, *321*, 385–388.

(7) Chae, H. K.; Siberio-Pérez, D. Y.; Kim, J.; Go, Y.; Eddaoudi, M.; Matzger, A. J.; O'Keeffe, M.; Yaghi, O. M. A Route to High Surface Area, Porosity, and Inclusion of Large Molecules in Crystals. *Nature* **2004**, *427*, 523–527.

(8) Morozov, S. V.; Novoselov, K. S.; Katsnelson, M. I.; Schedin, F.; Elias, D. C.; Jaszczak, J. A.; Geim, A. K. Giant Intrinsic Carrier Mobilities in Graphene and Its Bilayer. *Phys. Rev. Lett.* **2008**, *100*, 016602–1–016602–4.

(9) Rycerz, A.; Tworzydło, J.; Beenakker, C. W. J. Valley Filter and Valley Valve in Graphene. *Nat. Phys.* **2007**, *3*, 172–175.

(10) Allen, M. J.; Tung, V. C.; Kaner, R. B. Honeycomb Carbon: A Review of Graphene. *Chem. Rev.* **2010**, *110*, 132–145.

(11) Park, S.-W.; Lee, S.; Neuhauser, D. Geometry, Chemical Bonding, and Electronic Spectra of Si_n and Si_n–Glycine (*n* = 3–5) Complexes. *J. Phys. Chem. A* **2006**, *110*, 7173–7177. Chung, S.-Y.; Lee, S.; Liu, C.; Neuhauser, D. Structures and Electronic Spectra of CdSe–Cys Complexes: Density Functional Theory Study of a Simple Peptide-Coated Nanocluster. *J. Phys. Chem. B* **2009**, *113*, 292–301. Liu, C.; Chung, S.-Y.; Lee, S.; Weiss, S.; Neuhauser, D. Adsorbate-Induced Absorption Red Shift in an Organic–Inorganic Cluster Conjugate: Electronic Effects of Surfactants and Organic Adsorbates on the Lowest Excited States of a Methanethiol–CdSe Conjugate. *J. Chem. Phys.* **2009**, *131*, 174705–1–174705–8. Kim, H.-S.; Jang, S.-W.; Chung, S.-Y.; Lee, Y.; Kim, B.; Lee, S.; Liu, C.; Neuhauser, D. Effects of Bioconjugation on the Structures and Electronic Spectra of CdSe: Density Functional Theory Study of CdSe–Adenine Complexes. *J. Phys. Chem. B* **2010**, *114*, 471–479.

(12) Prezhdo, O.; Kamat, P. V.; Schatz, G. C. Virtual Issue: Graphene and Functionalized Graphene. *J. Phys. Chem. C* **2011**, *115*, 3195–3197.

(13) Du, A.; Smith, S. C. Electronic Functionality in Graphene-Based Nanoarchitectures: Discovery and Design via First-Principles Modeling. *J. Phys. Chem. Lett.* **2011**, *2*, 73–80.

(14) Lu, N.; Li, Z.; Yang, J. Electronic Structure Engineering via On-Plane Chemical Functionalization: A Comparison Study on Two-Dimensional Polysilane and Graphene. *J. Phys. Chem. C* **2009**, *113*, 16741–16746.

(15) Schniepp, H. C.; Li, J.-L.; McAllister, M. J.; Sai, H.; Herrera-Alonso, M.; Adamson, D. H.; Prud'homme, R. K.; Car, R.; Saville, D. A.; Aksay, I. A. Functionalized Single Graphene Sheets Derived from Splitting Graphite Oxide. *J. Phys. Chem. B* **2006**, *110*, 8535–8539.

(16) Lu, Y. H.; Chen, W.; Feng, Y. P.; He, P. M. Tuning the Electronic Structure of Graphene by an Organic Molecule. *J. Phys. Chem. B* **2009**, *113*, 2–5.

(17) Margine, E. R.; Bocquet, M.-L.; Blasé, X. Thermal Stability of Graphene and Nanotube Covalent Functionalization. *Nano Lett.* **2008**, *8*, 3315–3319.

(18) Wehling, T. O.; Novoselov, K. S.; Morozov, S. V.; Vdovin, E. E.; Katsnelson, M. I.; Geim, A. K.; Lichtenstein, A. I. Molecular Doping of Graphene. *Nano Lett.* **2008**, *8*, 173–177.

(19) Jiang, D.-e.; Sumpter, B. G.; Dai, S.; How Do Aryl Groups Attach to a Graphene Sheet? *J. Phys. Chem. B* **2006**, *110*, 23628–23632.

- (20) Al-Aqtash, N.; Vasiliev, I. Ab Initio Study of Carboxylated Graphene. *J. Phys. Chem. C* **2009**, *113*, 12970–12975.
- (21) Yang, Q.; Pan, X.; Clarke, K.; Li, K. Covalent Functionalization of Graphene with Polysaccharides. *Ind. Eng. Chem. Res.* **2012**, *51*, 310–317.
- (22) He, S.; Liu, K.-K.; Su, S.; Yan, J.; Mao, X.; Wang, D.; He, Y.; Li, L.-J.; Song, S.; Fan, C. Graphene-Based High-Efficiency Surface-Enhanced Raman Scattering-Active Platform for Sensitive and Multiplex DNA Detection. *Anal. Chem.* **2012**, *84*, 4622–4627.
- (23) Rochefort, A.; Wuest, J. D. Interaction of Substituted Aromatic Compounds with Graphene. *Langmuir* **2009**, *25*, 210–215.
- (24) Choi, J.; Kim, K.-j.; Kim, B.; Lee, H.; Kim, S. Covalent Functionalization of Epitaxial Graphene by Azidotrimethylsilane. *J. Phys. Chem. C* **2009**, *113*, 9433–9435.
- (25) Gao, X.; Jang, J.; Nagase, S. Hydrazine and Thermal Reduction of Graphene Oxide: Reaction Mechanisms, Product Structures, and Reaction Design. *J. Phys. Chem. C* **2010**, *114*, 832–842.
- (26) Charlier, J.-C.; Gonze, X.; Michenaud, J. P. First-Principles Study of Graphite Monofluoride (CF)_n. *Phys. Rev. B* **1993**, *47*, 16162–16168.
- (27) Takagi, Y.; Kusakabe, K. Transition from Direct Band Gap to Indirect Band Gap in Fluorinated Carbon. *Phys. Rev. B* **2002**, *65*, 121103–1–121103–4.
- (28) Boukhvalov, D. W. Stable Antiferromagnetic Graphene. *Physica E* **2010**, *43*, 199–201.
- (29) Cheng, S.-H.; Zou, K.; Okino, F.; Gutierrez, H. R.; Gupta, A.; Shen, N.; Eklund, P. C.; Sofo, J. O.; Zhu, J. Reversible Fluorination of Graphene: Evidence of a Two-Dimensional Wide Bandgap Semiconductor. *Phys. Rev. B* **2010**, *81*, 205435–1–205435–5.
- (30) Robinson, J. T.; Burgess, J. S.; Junkermeier, C. E.; Badescu, S. C.; Reinecke, T. L.; Perkins, F. K.; Zalalutdniov, M. K.; Baldwin, J. W.; Culbertson, J. C.; Sheehan, P. E.; Snow, E. S. Properties of Fluorinated Graphene Films. *Nano Lett.* **2010**, *10*, 3001–3005.
- (31) Stine, R.; Ciszek, J. W.; Barlow, D. E.; Lee, W.-K.; Robinson, J. T.; Sheehan, P. E. High-Density Amine-Terminated Monolayers Formed on Fluorinated CVD-Grown Graphene. *Langmuir* **2012**, *28*, 7957–7961.
- (32) Nair, R. R.; Ren, W.; Jalil, R.; Riaz, I.; Kravets, V. G.; Britnell, L.; Blake, P.; Schedin, F.; Mayorov, A. S.; Yuan, S.; Katsnelson, M. I.; Cheng, H.-M.; Strupinski, W.; Bulusheva, L. G.; Okotrub, A. V.; Grigorieva, I. V.; Grigorenko, A. N.; Novoselov, K. S.; Geim, A. K. Fluorographene: A Two-Dimensional Counterpart of Teflon. *Small* **2010**, *6*, 2877–2884.
- (33) Leenaerts, O.; Peelaers, H.; Hernandez-Nieves, A. D.; Partoens, B.; Peeters, F. M. First-Principles Investigation of Graphene Fluoride and Graphene. *Phys. Rev. B* **2010**, *82*, 195436–1–195436–6.
- (34) Withers, F.; Dubois, M.; Savchenko, A. K. Electron Properties of Fluorinated Single-Layer Graphene Transistors. *Phys. Rev. B* **2010**, *82*, 073403–1–073403–4.
- (35) Klintonberg, M.; Lebegue, S.; Katsnelson, M. I.; Eriksson, O. Theoretical Analysis of the Chemical Bonding and Electronic Structure of Graphene Interacting with Group IA and Group VIIA Elements. *Phys. Rev. B* **2010**, *81*, 085433–1–085433–5.
- (36) Yang, H.; Chen, M.; Zhou, H.; Qiu, C.; Hu, L.; Yu, F.; Chu, W.; Sun, S.; Sun, L. Preferential and Reversible Fluorination of Monolayer Graphene. *J. Phys. Chem. C* **2011**, *115*, 16844–16848.
- (37) Osuna, S.; Torrent-Sucarrat, M.; Solà, M.; Geerlings, P.; Ewels, C. P.; Van Lier, G. Reaction Mechanisms for Graphene and Carbon Nanotube Fluorination. *J. Phys. Chem. C* **2010**, *114*, 3340–3345.
- (38) Bon, S. B.; Valentini, L.; Verdejo, R.; Garcia Fierro, J. L.; Peponi, L.; Lopez-Manchado, M. A.; Kenny, J. M. Plasma Fluorination of Chemically Derived Graphene Sheets and Subsequent Modification With Butylamine. *Chem. Mater.* **2009**, *21*, 3433–3438.
- (39) Tang, S.; Zhang, S. Structural and Electronic Properties of Hybrid Fluorographene–Graphene Nanoribbons: Insight from First-Principles Calculations. *J. Phys. Chem. C* **2011**, *115*, 16644–16651.
- (40) Zhou, J.; Wu, M. M.; Zhou, X. Tuning Electronic and Magnetic Properties of Graphene by Surface Modification. *Appl. Phys. Lett.* **2009**, *95*, 103108–1–103108–3.
- (41) Şahin, H.; M. Topsakal, M.; Ciraci, S. Structures of Fluorinated Graphene and Their Signatures. *Phys. Rev. B* **2011**, *83*, 115432–1–115432–6.
- (42) Denis, P. A. Density Functional Investigation of Thioepoxidated and Thiolated Graphene. *J. Phys. Chem. C* **2009**, *113*, 5612–5619.
- (43) Samarakoon, D. K.; Chen, Z.; Nicolas, C.; Wang, X.-Q. Structural and Electronic Properties of Fluorographene. *Small* **2011**, *7*, 965–969.
- (44) Perdew, J. P.; Burke, K.; Ernzerhof, M. Generalized Gradient Approximation Made Simple. *Phys. Rev. Lett.* **1996**, *77*, 3865–3868.
- (45) Perdew, J. P.; Burke, K.; Ernzerhof, M. Erratum. *Phys. Rev. Lett.* **1997**, *78*, 1396–1396.
- (46) Blochl, P. E. Projector Augmented-Wave Method. *Phys. Rev. B* **1994**, *50*, 17953–17979. Kresse, G.; Joubert, D. From Ultrasoft Pseudopotentials to the Projector Augmented-Wave Method. *Phys. Rev. B* **1999**, *59*, 1758–1775.
- (47) Kresse, G.; Furthmüller, J. Efficient Iterative Schemes for Ab Initio Total Energy Calculations Using a Plane-Wave Basis Set. *Phys. Rev. B* **1996**, *54*, 11169–11186.
- (48) Kresse, G.; Hafner, J. Ab Initio Molecular Dynamics for Liquid Metals. *Phys. Rev. B* **1993**, *47*, 558–561.